Bol. Soc. Paran. Mat.
©SPM – E-ISSN-2175-1188
SPM: www.spm.uem.br/bspm

(3s.) **v. 2025 (43)** : 1–13.
ISSN-0037-8712
doi:10.5269/bspm.77807

Shear-Horizontal Wave Dynamics in Smart Fiber Composites with Layerwise Interfacial Imperfections

Bikram Dholey* and Kshitish Ch. Mistri

ABSTRACT: In this study, the propagation behavior of shear-horizontal (SH) waves in a tri-layered smart composite structure, including a piezoelectric fiber-reinforced composite (PFRC) core flanked by a fiber-reinforced composite (FRC) layer and a piezoelectric layer, is investigated. A crucial innovation of this work is the incorporation of suboptimal interfacial conditions, making the multilayered composite model more realistic. The dispersion relation for SH waves is determined analytically by constructing the governing equations and applying interfacial and boundary conditions. Numerical assessment of the connection indicates the effect of poor bonding on wave behavior. The impacts of interfacial bonding parameters and layer thickness ratios on SH wave phase velocity are investigated in depth parametrically. Results show that wave propagation is highly influenced by interfacial properties and geometric configurations, therefore stressing important design issues for uses in structural health monitoring, energy harvesting, and nondestructive evaluation. For advanced multilayer composite systems, this study offers a unique analytical structure and insightful design ideas.

Key Words: SH-wave propagation, Fiber-reinforced composite (FRC), Piezoelectric fiber-reinforced composite (PFRC), Piezoelectric layer, Classical Spring

Contents

1. Introduction

Fiber-reinforced composites (FRCs) have become essential materials in contemporary engineering because they are very strong for their weight, last a long time, and can withstand severe environments [11, 1]. These qualities make FRCs perfect for use in high-performance settings in the aerospace, automotive, civil infrastructure, and other fields.

Piezoelectric fiber-reinforced composites (PFRCs) represent a significant advancement in smart material technology. PFRCs combine the structural strength of typical fiber-reinforced composites (FRCs) with the unique capacity to sense mechanical changes and collect energy from the environment by adding piezoelectric phases to them [7,12,20]. This hybrid design not only makes the material stronger, but it also allows for strong electromechanical coupling, which is better than what traditional monolithic

* Corresponding author.

Submitted July 11, 2025. Published September 23, 2025
2020 *Mathematics Subject Classification:* 35A18, 35L05, 74J05.

piezoelectric materials can do in terms of durability and energy output [18]. Because of these many uses, PFRCs are now necessary for a lot of modern technologies, such as structural health monitoring (SHM) systems, microelectromechanical systems (MEMS), precision actuators, underwater acoustic transducers, and biomedical implants and sensors [13,2,6].

Shear horizontal (SH) waves are especially helpful in wave mechanics for the study of multilayer composites like PFRCs. Due to their in-plane polarization, SH waves interact distinctively with multilayer structures, making them useful for measuring mechanical and electrical reactions [3]. Studying their propagation in layered media—such as PFRCs between FRC layers and piezoelectric substrates—offers insights into wave speed, energy attenuation, and design optimization for wave-based applications [14,4].

Despite improvements, the importance of defective interfaces in multilayer composites remains underexplored. Interfaces often store flaws like voids, debonding, or fractures, which disturb mechanical and electrical continuity. These defects modify stress transmission, limit output efficiency, and influence SH wave behavior considerably [17,26]. Although some work has addressed the effect of loosely bound interfaces on elastic wave propagation [24,16,21,10,8,25], more research is needed, especially in layered PFRC systems.

Emphasizing the impact of interfacial defects on wave behavior and energy transmission, this work investigates SH-wave propagation through a layered system including an FRC, a PFRC, and a piezoelectric substrate.

This study seeks a double-edged purpose. First, we construct a mathematical framework for a smart, layered composite structure consisting of a top fiber-reinforced composite (FRC) layer, a bottom piezoelectric substrate, and an intermediate piezoelectric fiber-reinforced composite (PFRC) layer. To increase physical realism, the model contains spring-type imperfect interfaces between neighboring layers, representing the effects of interfacial compliance.

Second, we analyze the dispersion properties of shear horizontal (SH) waves traveling through this structure. Specifically, we study how wave behavior is impacted by differences in layer thickness ratios and the stiffness of the interfacial springs. This research gives crucial insights into the dynamic behavior of multifunctional composites and underlines the relevance of imperfect bonding in wave-based sensing and energy applications.

2. Problem Formulation

We study a smart composite tri-layered structure having three unique layers:

- A fiber-reinforced composite (FRC) layer of thickness $H_1 - H_2$, positioned at the top,
- A piezoelectric fiber-reinforced composite (PFRC) layer of thickness $H_2 - H_3$, placed in the middle, and
- A piezoelectric layer of thickness H_3, located at the bottom.

To represent this structure, we create a Cartesian coordinate system (x, y, z), with the x-axis aligned along the bottom border of the piezoelectric layer. This axis also acts as the direction of polarization, as indicated in Fig. 1.

The strata are identified using superscripts:

- Superscript $'$ for the upper FRC layer,
- Superscript $''$ for the middle PFRC layer, and
- Superscript $'''$ for the bottom piezoelectric layer.

Under the assumption of plane strain conditions, the displacement components are written as functions of x and y only. This formulation provides a concentrated investigation of wave propagation and electromechanical interactions inside the layered smart structure.

For the propagation of shear horizontal (SH) waves, the displacement is thought to occur normal to the xy-plane, i.e., along the z-direction. As a result, the in-plane displacement components vanish in all three layers. The displacement fields are consequently represented as: $u_1^{'} = u_2^{'} = 0, u_3^{'} = u_3^{'}(x, y, t)$, (in

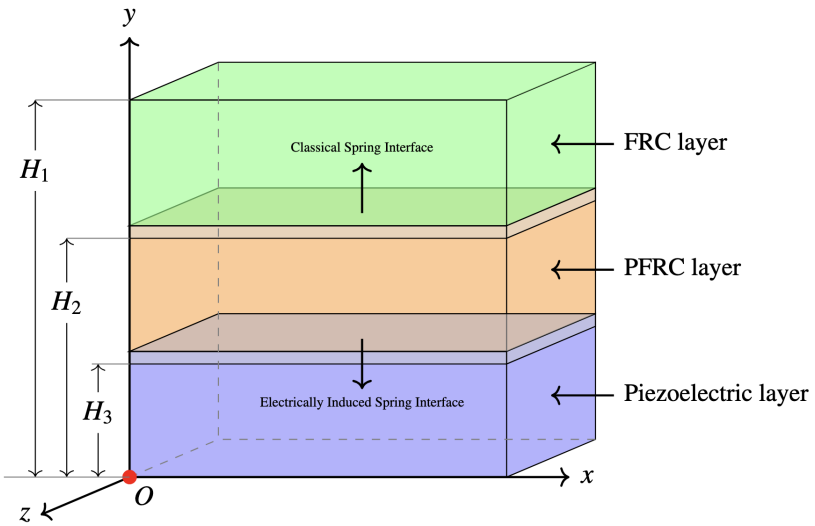

Figure 1: Schematic illustration of the proposed model.

the upper FRC layer), $u_1^{''} = u_2^{''} = 0, u_3^{''} = u_3^{''}(x, y, t)$(in the middle PFRC layer), $u_1^{'''} = u_2^{'''} = 0, \quad u_3^{'''} = u_3^{'''}(x, y, t)$(in the bottom piezoelectric layer).

In addition, due to the electromechanical nature of the intermediate and bottom layers, the electric potentials are specified as:

$$\phi^{''} = \phi^{''}(x, y, t), \quad \phi^{'''} = \phi^{'''}(x, y, t),$$

for the PFRC and piezoelectric layers, respectively.

3. Constitutive Relations and Analytical Solutions

In this part, we obtain the constitutive equations and accompanying analytical solutions for each of the three layers in the composite structure: the top fiber-reinforced composite (FRC) layer, the middle piezoelectric fiber-reinforced composite (PFRC) layer, and the bottom piezoelectric layer.

3.1. Top FRC layer

Following the work by Singh et al. [23], the constitutive relation for the fiber-reinforced composite (FRC) layer in a preferred direction $\vec{a} = (a_1, a_2, a_3)$ with the constraint $a_1^2+a_2^2+a_3^2 = 1$ may be represented in vector form as:

$$\tau_{ij}^{'} = \lambda e_{ll}^{'}\delta_{ij} + 2\mu_T e_{ij}^{'} + \alpha\left(a_l a_m e_{lm}^{'}\delta_{ij} + a_i a_j e_{ll}^{'}\right) + 2(\mu_L - \mu_T)\left(a_i a_l e_{lj}^{'} + a_j a_l e_{li}^{'}\right) + \beta\left(a_l a_m e_{lm}^{'} a_i a_j\right), \tag{3.1}$$

where $i, j, l, m = 1, 2, 3$. In this equation $\tau_{ij}^{'}$ are the stress components, $e_{ij}^{'}$ are the infinitesimal strain components, μ_T and μ_L are the transverse and longitudinal shear moduli, λ is the Lamé constant, α and β are extra elastic constants, δ_{ij} is the Kronecker delta.

The equation of motion in the absence of body forces is [9]:

$$\partial_x \tau_{31}^{'} + \partial_y \tau_{32}^{'} = \rho_1 \partial_{tt} u_3^{'}, \tag{3.2}$$

where ρ_1 is the mass density of the FRC layer.

Substituting Eq. (3.1) into Eq. (3.2), we obtain the governing differential equation as:

$$\mu_T \partial_{xx} u_3^{'} + (\mu_L - \mu_T)\left(a_1^2 \partial_{xx} u_3^{'} + a_1 a_2 \partial_{xy} u_3^{'}\right) + \mu_T \partial_{yy} u_3^{'} + (\mu_L - \mu_T)\left(a_2 a_1 \partial_{yx} u_3^{'} + a_2^2 \partial_{yy} u_3^{'}\right) = \rho_1 \partial_{tt} u_3^{'}. \tag{3.3}$$

To solve Eq. (3.3), we assume a time-harmonic and spatially dependent solution of the form:

$$u_3^{'} = b_1(y)\ \mathrm{e}^{ik(x-ct)}, \tag{3.4}$$

where k is the wave number and c is the phase velocity.

Substituting Eq. (3.4) into Eq. (3.3) and simplifying under the assumption of sinusoidal wave motion produces the displacement solution:

$$u_3^{'} = \mathrm{e}^{-M_1 y/2}\left(A_1 \cos\left(\frac{\sqrt{M_1^2-4M_2}}{2}y\right) + A_2 \sin\left(\frac{\sqrt{M_1^2-4M_2}}{2}y\right)\right)\mathrm{e}^{ik(x-ct)} \tag{3.5}$$

Here, A_1 and A_2 are integration constants, and the equations for M_1 and M_2 are presented in the Appendix.

3.2. Sandwiched PFRC layer

The studied piezoelectric fiber-reinforced composite (PFRC) layer comprises of a piezoelectric fiber (PZT-5H) inserted in a non-piezoelectric epoxy matrix. The constitutive relations guiding the behavior of the PFRC material are [9]:

$$\tau_{ij}^{''} = [c_{ij}^{''}]\{\epsilon_{ij}^{''}\} - [e_{ij}^{''}]^T\{E_i^{''}\} \tag{3.6}$$

$$D_{ij}^{''} = [e_{ij}^{''}]\{\epsilon_{ij}^{''}\} + [\zeta_{ij}^{''}]^T\{E_i^{''}\} \tag{3.7}$$

where, $\tau_{ij}^{''} = \begin{bmatrix} \tau_{11}^{''} \\ \tau_{22}^{''} \\ \tau_{33}^{''} \\ \tau_{23}^{''} \\ \tau_{13}^{''} \\ \tau_{12}^{''} \end{bmatrix}$, $\{\epsilon_{ij}^{''}\} = \begin{bmatrix} \epsilon_{11}^{''} \\ \epsilon_{22}^{''} \\ \epsilon_{33}^{''} \\ 2\epsilon_{23}^{''} \\ 2\epsilon_{13}^{''} \\ 2\epsilon_{12}^{''} \end{bmatrix}$, $D_{ij}^{''} = \begin{bmatrix} D_1^{''} \\ D_2^{''} \\ D_3^{''} \end{bmatrix}$, $\{\mathrm{E}_i^{''}\} = \begin{bmatrix} E_1^{''} \\ E_2^{''} \\ E_3^{''} \end{bmatrix}$,

$$[c_{ij}^{''}] = \begin{bmatrix} c_{11}^{''} & c_{12}^{''} & c_{13}^{''} & 0 & 0 & 0 \\ c_{12}^{''} & c_{22}^{''} & c_{23}^{''} & 0 & 0 & 0 \\ c_{13}^{''} & c_{23}^{''} & c_{33}^{''} & 0 & 0 & 0 \\ 0 & 0 & 0 & c_{44}^{''} & 0 & 0 \\ 0 & 0 & 0 & 0 & c_{44}^{''} & 0 \\ 0 & 0 & 0 & 0 & 0 & c_{66}^{''} \end{bmatrix}, [\mathrm{e}_{ij}^{''}]^T = \begin{bmatrix} 0 & 0 & e_{13}^{''} \\ 0 & 0 & e_{32}^{''} \\ 0 & 0 & e_{33}^{''} \\ 0 & e_{15}^{''} & 0 \\ e_{15}^{''} & 0 & 0 \\ 0 & 0 & 0 \end{bmatrix}, [\zeta_{ij}^{''}] = \begin{bmatrix} \zeta_{11}^{''} & 0 & 0 \\ 0 & \zeta_{22}^{''} & 0 \\ 0 & 0 & \zeta_{33}^{''} \end{bmatrix}.$$

and $\tau_{ij}^{''}$ is the stress tensor, $c_{ij}^{''}$ are the elastic constants, $\epsilon_{ij}^{''} = \frac{1}{2}(\partial_j u_i + \partial_i u_j)$ is the infinitesimal strain tensor, $e_{ij}^{''}$ are the piezoelectric constants, $E_i^{''} = -\partial_i \phi^{''}$ signifies the electric field vector obtained from the electric potential $\phi^{''}$, $D_i^{''}$ are the electric displacement components, $\zeta_{ij}^{''}$ are the dielectric constants.

The epoxy matrix, being piezoelectrically inert, has $e_{ij} = 0$. The effective constitutive characteristics of the PFRC are derived using strength of materials and rule of mixtures approaches [8]. The total response of the PFRC depends on the characteristics of PZT-5H, epoxy, and the volume percentage of piezoelectric fibers V^f. By adjusting V^f, the effective parameters may be customized for individual technical needs.

Following [5], the equations of motion for the PFRC layer are:

$$\begin{aligned} \partial_x \tau_{13}^{''} + \partial_y \tau_{23}^{''} &= \rho_2\, \partial_{tt} u_3^{''}, \\ \partial_x D_1^{''} + \partial_y D_2^{''} &= 0, \end{aligned} \tag{3.8}$$

where ρ_2 is the mass density of the PFRC layer. Substituting the constitutive expressions from Eqs. (3.6)–(3.7) into Eq. (3.8), one can have

$$\begin{aligned} c_{44}^{''}\partial_{xx}u_3^{''} + c_{44}^{''}\partial_{yy}u_3^{''} + e_{15}^{''}\left(\partial_{xx}\phi^{''} + \partial_{yy}\phi^{''}\right) &= \rho_2\,\partial_{tt}u_3^{''} \\ e_{15}^{''}\left(\partial_{xx}u_3^{''} + \partial_{yy}u_3^{''}\right) - \zeta_{11}^{''}\left(\partial_{xx}\phi^{''} + \partial_{yy}\phi^{''}\right) &= 0 \end{aligned} \tag{3.9}$$

Assume time-harmonic and spatially dependent solutions for the mechanical displacement and electric potential of the PFRC layer as:

$$[u_3^{''}, \phi^{''}] = [b_2(y), \phi_2(y)]\,\mathrm{e}^{ik(x-ct)} \tag{3.10}$$

Substituting these into Eq. (3.9) produces the explicit solutions:

$$\begin{aligned} u_3^{''} &= (A_3\cos(ry) + A_4\sin(ry))\ \mathrm{e}^{ik(x-ct)} \\ \phi^{''} &= \left[A_5\,\mathrm{e}^{ky} + A_6\,\mathrm{e}^{-ky} + \frac{e_{15}^{''}}{\zeta_{11}^{''}}\left(A_3\cos(ry) + A_4\sin(ry)\right)\right]\ \mathrm{e}^{ik(x-ct)} \end{aligned} \tag{3.11}$$

Here, A_3, A_4, A_5, and A_6 are arbitrary constants, and r is specified in the Appendix.

3.3. Bottom piezoelectric layer

The lower piezoelectric layer is considered as a transversely isotropic type. According to [22], the constitutive relations for this layer are represented as:

$$\begin{aligned} \tau_{11}^{'''} &= c_{11}^{'''}\epsilon_{11}^{'''} + c_{12}^{'''}\epsilon_{22}^{'''} + c_{13}^{'''}\epsilon_{33}^{'''} - e_{31}^{'''}E_3^{'''} \\ \tau_{22}^{'''} &= c_{12}^{'''}\epsilon_{11}^{'''} + c_{11}^{'''}\epsilon_{22}^{'''} + c_{13}^{'''}\epsilon_{33}^{'''} - e_{31}^{'''}E_3^{'''} \\ \tau_{33}^{'''} &= c_{13}^{'''}(\epsilon_{11}^{'''} + \epsilon_{22}^{'''}) + c_{33}^{'''}\epsilon_{33}^{'''} - e_{33}^{'''}E_3^{'''} \\ \tau_{23}^{'''} &= 2c_{44}^{'''}\epsilon_{23}^{'''} - e_{15}^{'''}E_2^{'''} \\ \tau_{31}^{'''} &= 2c_{44}^{'''}\epsilon_{31}^{'''} - e_{15}^{'''}E_1^{'''} \\ \tau_{12}^{'''} &= (c_{11}^{'''} - c_{12}^{'''})\epsilon_{12}^{'''} \\ D_1^{'''} &= 2e_{15}^{'''}\epsilon_{31}^{'''} + \zeta_{11}^{'''}E_1^{'''} \\ D_2^{'''} &= 2e_{15}^{'''}\epsilon_{23}^{'''} + \zeta_{11}^{'''}E_2^{'''} \\ D_3^{'''} &= e_{31}^{'''}(\epsilon_{11}^{'''} + \epsilon_{22}^{'''}) + e_{33}^{'''}\epsilon_{33}^{'''} + \zeta_{33}^{'''}E_3^{'''} \end{aligned} \tag{3.12}$$

The governing equations of motion for the piezoelectric medium, in the absence of body forces, are stated as [**?**]:

$$\begin{aligned} \partial_x\tau_{31}^{'''} + \partial_y\tau_{32}^{'''} &= \rho_3\,\partial_{tt}u_3^{'''}, \\ \partial_x D_1^{'''} + \partial_y D_2^{'''} &= 0, \end{aligned} \tag{3.13}$$

where ρ_3 is the mass density of the piezoelectric layer. Following the technique in Section 3.2, we assume time-harmonic and space-dependent solutions of the form:

$$[u_3^{'''}, \phi^{'''}] = [b_3(y), \phi_3(y)]\,\mathrm{e}^{ik(x-ct)}$$

Substituting this into Eq. (3.13), we obtain the general solutions for the displacement and electric potential as:

$$u_3^{'''} = \left(A_7\,\mathrm{e}^{sy} + A_8\,\mathrm{e}^{-sy}\right)\ \mathrm{e}^{ik(x-ct)} \tag{3.14}$$

$$\phi''' = \left(\left(A_7 n\,\mathrm{e}^{sy} + A_8 n\,\mathrm{e}^{-sy} + A_9\,\mathrm{e}^{ky} + \Gamma_{10}\,\mathrm{e}^{-ky}\right)\right)\mathrm{e}^{ik(x-ct)} \tag{3.15}$$

Here, A_7, A_8, A_9, A_{10} are arbitrary constants, while the parameters s and n are specified in the Appendix.

Table 1: Carbon fibre-epoxy resin composite material characteristics specified in FRC medium [5].

Material data	FRC
Elastic constants ($\times 10^{10}$ N/m^2)	$\mu_L = 5.66$, $\mu_T = 2.46$
Density (kg/m^3)	$\rho_1 = 3321$

4. Boundary Conditions

The upper boundary (at $y = H_1$) of the FRC layer is traction-free, i.e.,

$$\tau_{23}^{'} = 0 \tag{4.1}$$

Based on Hooke's law, which states that stress is proportional to strain in elastic materials, the interfacial behavior between the FRC and PFRC layers is modeled using a linear spring condition. The common interface of FRC and PFRC layers has an imperfection due to the presence of classical spring interface (at $y = H_2$)

$$\tau_{23}^{'} = \tau_{23}^{''} = \bar{\alpha}_1(u_3^{''} - u_3^{'}), \tag{4.2}$$

$$\phi^{''} = 0, \tag{4.3}$$

where $\bar{\alpha}_1 \geq 0$ is the mechanical spring constant with dimension of N/m^3. At the common interface of the PFRC layer and the piezoelectric layer (ie, $y = H_3$) due to the presence of a classical electrically induced spring layer, the boundary conditions are:

$$\tau_{23}^{'''} = \tau_{23}^{''} = \bar{\alpha}_2(u_3^{''} - u_3^{'''}) \tag{4.4}$$

$$D_2^{'''} = D_2^{''} = \bar{\alpha}_3(\phi^{''} - \phi^{'''}) \tag{4.5}$$

where $\bar{\alpha}_2 \geq 0$ and $\bar{\alpha}_3 \geq 0$ are the mechanical and electrical spring constants that have a dimension of N/m^3.

Moreover, the lower boundary of the piezoelectric layer is traction-free and electrically bounded at $y = 0$. Thus, these give two additional boundary conditions as follows

$$\tau_{23}^{'''} = 0 \tag{4.6}$$

$$\phi^{'''} = 0 \tag{4.7}$$

Substituting the electromechanical expressions in the above boundary conditions, we obtain a set of equations describing the system's behavior. These equations are provided in matrix form as follows

$$\Gamma A = 0 \tag{4.8}$$

where, Γ is a square matrix of order 10 listed in Appendix and A=$[A_1 \dots A_{10}]^T$. Then, finding the determinant of the above matrix Γ and expanding the resulting equation leads to the dispersion relation of the propagating SH-wave in the layered structure comprising a PFRC layer sandwiched between an upper mechanically bonded FRC layer and a lower electro-mechanically bonded piezoelectric layer.

5. Numerical analysis

This article anticipate how bonding factors, and thickness ratios affect the speed of SH waves in a system with more than one layer. This study considered three materials: carbon fiber-epoxy (FRC, Table 1), PZT-5H/epoxy (PFRC, Table 2), and PVDF (piezoelectric layer, Table 3).

Table 2: The PZT-5H - epoxy material characteristics specified for PFRC layer [15,5].

Material data	PZT-5H	Epoxy
Elastic constant ($\times 10^9$ N/m^2)	$c_{44} = 23$	$c_{44} = 2.57$
Piezoelectric constant (C/m^2)	$e_{15} = 17$	$e_{15} = 0$
Dielectric constant ($\times 10^{-9} F/m$)	$\zeta_{11} = 15.05$	$\zeta_{11} = 0.079$
Density (kg/m^3)	$\rho_2 = 5407$	$\rho_2 = 1210$

Table 3: Polyvinylidene fluoride material characteristics specified for the piezoelectric layer [22].

Material data	PVDF
Elastic constants ($\times 10^{10} N/m^2$)	$c'''_{44} = 0.91$
Piezoelectric constants (C/m^2)	$e'''_{15} = -0.16$
Dielectric constants($\times 10^{-10} F/m$)	$\zeta'''_{11} = 1.062$
Density (kg/m^3)	$\rho_3 = 1780$

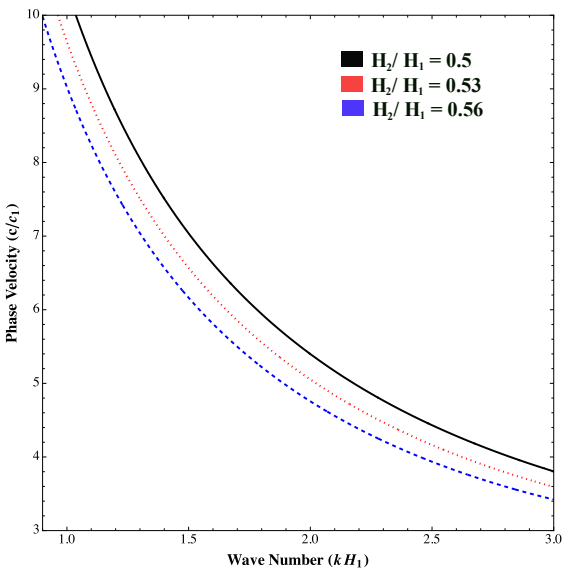

Figure 2: Effect of thickness ratio H_2/H_1 on the normalized phase velocity c/c_1 as a function of wave number kH_1. An increase in H_2/H_1 leads in a constant fall in phase velocity.

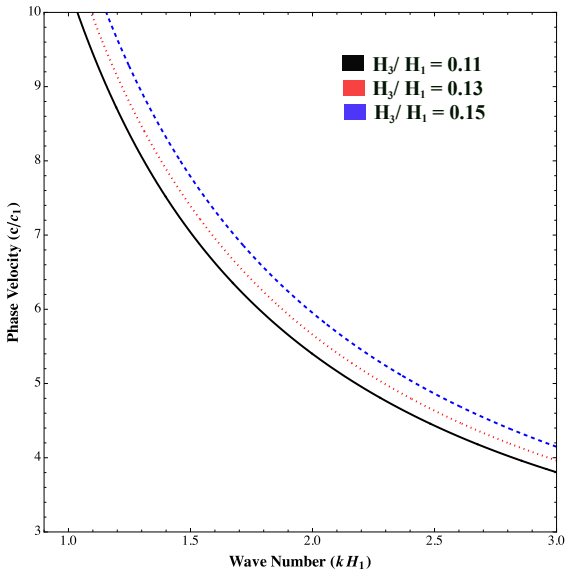

Figure 3: Effect of thickness ratio H_2/H_1 on the normalized phase velocity c/c_1 as a function of wave number kH_1. An increase in H_3/H_1 leads in a constant increase in phase velocity.

5.1. Impact of thickness ratio on phase velocity

Fig. 2 shows the fluctuation of normalized phase velocity c/c_1 with regard to the non-dimensional wave number kH_1 for different values of the thickness ratio H_2/H_1. The phase velocity goes down steadily throughout all wave numbers as H_2/H_1 goes from 0.50 (black solid line) to 0.56 (blue dash-dot line). For all situations, the phase velocity displays a monotonically declining trend with increasing kH_1, showing dispersive wave behavior. An increase in the thickness ratio H_2/H_1 leads to a drop in phase velocity, underlining the relevance of geometric configuration in influencing wave propagation in layered composite systems.

Fig. 3 depicts the influence of the top layer thickness ratio H_3/H_1 on the normalized phase velocity c/c_1 with regard to the wave number kH_1. As the ratio H_3/H_1 grows from 0.11 (black solid line) to 0.15 (blue dash-dot line), the phase velocity rises over the whole wave number range. This tendency gets more prominent with higher wave numbers. A greater value of H_3/H_1 raises the phase velocity, underlining the critical importance of the upper layer's thickness in modulating wave propagation in composite layered systems.

5.2. Impact of bonding parameters on phase velocity

Fig. 4 indeicates the impact of the interfacial parameter α_1 on the normalized phase velocity c/c_1 as a function of the wave number kH_1. As α_1 climbs from 0 (green dashed line), typifying the case of a waveguide to 1×10^{10} (blue dash-dot line), the phase velocity increases for all values of kH_1. This tendency shows that increased interfacial coupling raises the effective stiffness of the structure, hence permitting quicker SH-wave propagation. The dispersion effect is obvious across all scenarios, with velocity dropping as wave number increases. The impact of α_1 is more obvious with higher wave numbers. An increase in α_1 considerably raises phase velocity, indicating the crucial importance of interfacial bonding in modifying wave properties in composite layered systems.

Fig. 5 depicts the influence of the interfacial parameter α_2 on the normalized phase velocity c/c_1 as a function of the wave number kH_1. As α_2 climbs from 0 (green dashed line), typifying the case of a waveguide to 1×10^{10} (blue dash-dot line), the phase velocity demonstrates a substantial rise across all wave numbers. The rising trend of phase velocity with respect to α_2 suggests that higher bonding strength at the relevant interface greatly enhances the structural stiffness, hence facilitating quicker shear-horizontal wave propagation. The dispersion characteristic, as observed by the decreasing phase velocity

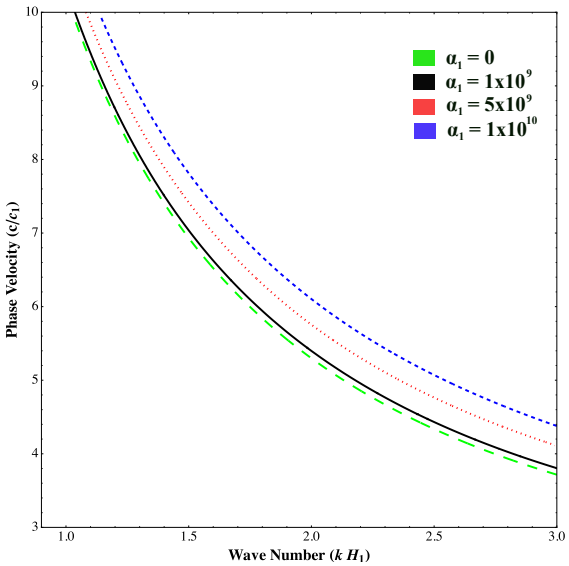

Figure 4: Effect of spring constant α_1 on the normalized phase velocity c/c_1 as a function of wave number kH_1. An increase in α_1 leads in a constant increase in phase velocity.

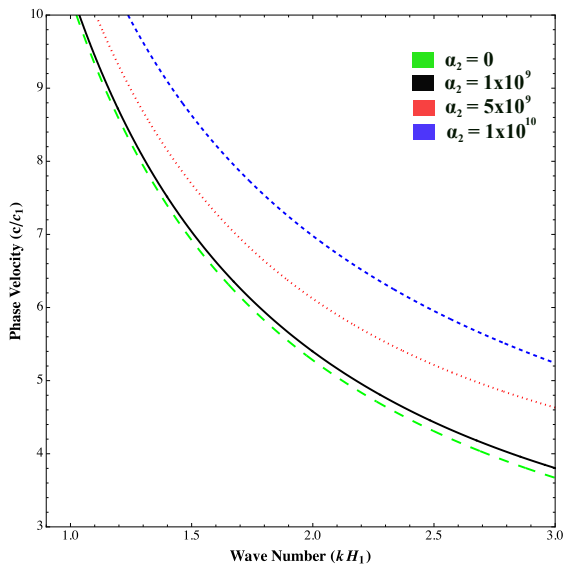

Figure 5: Effect of mechanical spring constant α_2 on the normalized phase velocity c/c_1 as a function of wave number kH_1. An increase in α_2 leads in a constant increase in phase velocity.

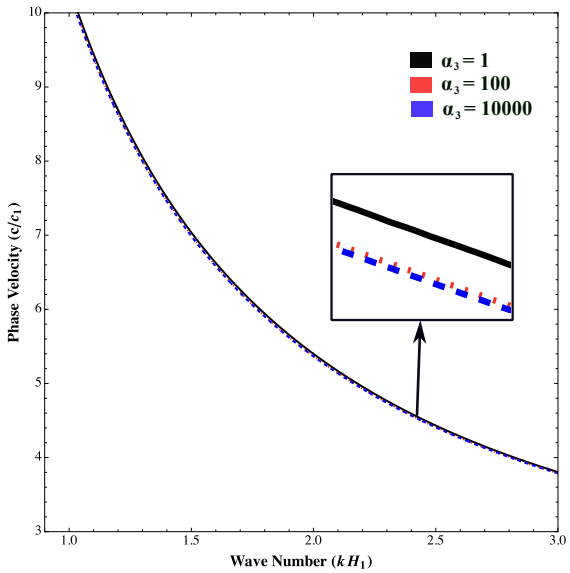

Figure 6: Effect of electric spring constant α_3 on the normalized phase velocity c/c_1 as a function of wave number kH_1. An increase in α_3 leads slight fall in phase velocity.

with rising kH_1, stays clear in each situation. Increasing α_2 leads to a larger phase velocity, supporting the crucial function of interfacial bonding in regulating wave transmission in layered composite media.

Fig. 6 shows the fluctuation of normalized phase velocity c/c_1 with wave number kH_1 for different values of the bonding parameter α_3. The curves for $\alpha_3 = 1$, 100, and 10000 illustrate that the phase velocity displays only a small sensitivity to changes in α_3. However, a slight but apparent variation emerges with higher wave numbers, as noted in the zoomed-in inset. The blue (dash-dot) and red (dotted) curves corresponding to higher α_3 values tend to display somewhat lower phase velocities compared to the black solid line ($\alpha_3 = 1$).

The electric spring constant α_3 has a slight impact on SH-wave propagation, especially visible at higher wave numbers, demonstrating its relatively limited control over the overall dispersion behavior.

Fig. 6 shows the fluctuation of normalized phase velocity c/c_1 with wave number kH_1 for different values of the bonding parameter α_3. The curves for $\alpha_3 = 1$, 100, and 10000 illustrate that the phase velocity displays only a small sensitivity to changes in α_3. However, a slight but apparent variation emerges with higher wave numbers, as noted in the zoomed-in inset. The blue (dash-dot) and red (dotted) curves corresponding to higher α_3 values tend to display somewhat lower phase velocities compared to the black solid line ($\alpha_3 = 1$).

The electric spring constant α_3 has a slight impact on SH-wave propagation, especially visible at higher wave numbers, demonstrating its relatively limited control over the overall dispersion behavior.

6. Conclusion

This work analyzes the impact of different geometric and interfacial characteristics on the phase velocity of shear-horizontal (SH) waves in a layered composite structure. An increase in the intermediate layer thickness ratio H_2/H_1 leads to a constant decrease in phase velocity, suggesting a reduction in overall structural stiffness. Conversely, raising the top layer thickness ratio H_3/H_1 resulted in greater phase velocities, implying improved stiffness and quicker wave propagation. Furthermore, the interfacial spring constants α_1 and α_2, indicating mechanical bonding strength at distinct surfaces, considerably raise the phase velocity with increasing values, underlining the crucial role of interfacial coupling in wave modulation. In contrast, the electric bonding parameter α_3 exerts only a tiny reverse impact, especially visible at higher wave numbers. Overall, the findings underscore that both geometric configuration and interfacial bonding conditions play pivotal roles in controlling SH-wave dispersion in layered composite

media, offering valuable insights for the design and optimization of advanced waveguide systems and smart composite structures.

Acknowledgment

The author is grateful to his respective institution for providing the best facilities to carry out this research work.

References

1. HM Abo-Bakr, RM Abo-Bakr, RA Shanab, and MA Eltaher. Optimal material and geometry of 2d-fgm tapered microbeams under dynamic and static constraints. *Mechanics Based Design of Structures and Machines*, 52(8):5227–5262, 2024.

2. E Koray Akdogan, Mehdi Allahverdi, and Ahmad Safari. Piezoelectric composites for sensor and actuator applications. *IEEE transactions on ultrasonics, ferroelectrics, and frequency control*, 52(5):746–775, 2005.

3. Bertram Alexander Auld. *Acoustic fields and waves in solids*. Ripol Klassik Publishing, 1973.

4. Colin Campbell. *Surface acoustic wave devices and their signal processing applications*. Elsevier, 2012.

5. Amrita Das, Abhishek Kumar Singh, Prajnya Parimita Patel, Kshitish Ch. Mistri, and Amares Chattopadhyay. Reflection and refraction of plane waves at the loosely bonded common interface of piezoelectric fibre-reinforced and fibre-reinforced composite media. *Ultrasonics*, 94:131–144, 2019.

6. Aman Garg, Li Li, and Anshu Sharma. Free vibration analysis of bio-inspired double-and cross-helicoidal laminated composite plates. *Mechanics Based Design of Structures and Machines*, pages 1–17, 2024.

7. Ronald F Gibson. A review of recent research on mechanics of multifunctional composite materials and structures. *Composite structures*, 92(12):2793–2810, 2010.

8. Sayantan Guha and Abhishek Kumar Singh. Plane wave reflection/transmission in imperfectly bonded initially stressed rotating piezothermoelastic fiber-reinforced composite half-spaces. *European Journal of Mechanics-A/Solids*, 88:104242, 2021.

9. Sayantan Guha and Abhishek Kumar Singh. Transference of sh waves in a piezoelectric fiber-reinforced composite layered structure employing perfectly matched layer and infinite element techniques coupled with finite elements. *Finite Elements in Analysis and Design*, 209:103814, 2022.

10. Xiao Guo, Peijun Wei, Li Li, and Qiheng Tang. Influences of mechanically and dielectrically imperfect interfaces on the reflection and transmission waves between two piezoelectric half spaces. *International Journal of Solids and Structures*, 63:184–205, 2015.

11. MJKA Hinton. *Failure criteria in fibre reinforced polymer composites: the world-wide failure exercise*. Elsevier, 2004.

12. Armagan Karamanli, Thuc P Vo, and Mohamed A Eltaher. Transient analysis of bio-inspired shear and normal deformable laminated composite plates using a higher-order finite element model. *Mechanics Based Design of Structures and Machines*, pages 1–25, 2024.

13. Seth Stovack Kessler. *Piezoelectric-based in-situ damage detection of composite materials for structural health monitoring systems*. PhD thesis, Massachusetts Institute of Technology, 2002.

14. Gordon S Kino. Acoustic waves: devices, imaging, and analog signal processing. *(No Title)*, 1987.

15. Anil Kumar and D Chakraborty. Effective properties of thermo-electro-mechanically coupled piezoelectric fiber reinforced composites. *Materials & Design*, 30(4):1216–1222, 2009.

16. Anton I Lavrentyev and SI Rokhlin. Ultrasonic spectroscopy of imperfect contact interfaces between a layer and two solids. *The Journal of the Acoustical Society of America*, 103(2):657–664, 1998.

17. GS1880195 Murty. A theoretical model for the attenuation and dispersion of stoneley waves at the loosely bonded interface of elastic half spaces. *Physics of the Earth and Planetary Interiors*, 11(1):65–79, 1975.

18. Adnan H Nayfeh. *Wave propagation in layered anisotropic media: With application to composites*. Elsevier, 1995.

19. T.T. Nguyen, R. Abdelmoula, J. Li, Y. Roussigne, and A. Stashkevich. Wave propagating in multilayers composed of piezo electric and piezo magnetic layers. *Composites Part B: Engineering*, 93:289–301, 2016.

20. Mahsa Pahlavanzadeh, Mehdi Mohammadimehr, Mohsen Irani-Rahaghi, and Seyed Mojtaba Emamat. Vibration response on the rod of vortex bladeless wind power generator for a sandwich beam with various face sheets and cores based on different boundary conditions. *Mechanics Based Design of Structures and Machines*, pages 1–27, 2024.

21. SI Rokhlin and YJ Wang. Analysis of boundary conditions for elastic wave interaction with an interface between two solids. *The Journal of the Acoustical Society of America*, 89(2):503–515, 1991.

22. Amrita Das Sharmistha Rakshit, Kshitish Ch. Mistri and Anirban Lakshman. Effect of interfacial imperfections on sh-wave propagation in a porous piezoelectric composite. *Mechanics of Advanced Materials and Structures*, 29(25):4008–4018, 2022.

23. A. K. Singh, K. C. Mistri, and A. Das. Propagation of love-type wave in a corrugated fibre-reinforced layer. *Journal of Mechanics*, 32(6):693–708, 2016.

24. AK Singh, Z Parween, A Das, and A Chattopadhyay. Influence of loosely-bonded sandwiched initially stressed visco-elastic layer on torsional wave propagation. *Journal of Mechanics*, 33(3):351–368, 2017.

25. Sonam Singh, AK Singh, and Sayantan Guha. Impact of interfacial imperfections on the reflection and transmission phenomenon of plane waves in a porous-piezoelectric model. *Applied Mathematical Modelling*, 100:656–675, 2021.

26. AK Vashisth, MD Sharma, and ML Gogna. Reflection and transmission of elastic waves at a loosely bonded interface between an elastic solid and liquid-saturated porous solid. *Geophysical journal international*, 105(3):601–617, 1991.

Appendix

• Terms in the mechanical displacement $u_3^{'}$ top FRC layer:
$M_1 = [2ik\ a_1\ a_2(\mu_L - \mu_T)]/[\mu_T + (\mu_L - \mu_T)a_2^2]$
$M_2 = [k^2(\rho_1 c^2 - \mu_T - (\mu_L - \mu_T)a_1^2)]/[\mu_T + (\mu_L - \mu_T)a_2^2]$ and $c_1 = \sqrt{\mu_T/\rho_1}$ denotes the phase velocity in the FRC layer. • Terms in the mechanical displacement $u_3^{''}$ and electric potential $\phi^{''}$ of the sandwiched PFRC layer:

$r = k\sqrt{\frac{c^2}{c_2^2} - 1}$, where c_2 denotes the phase velocity in the PFRC layer and is given by $c_2 = \sqrt{\frac{c_{44}^{''} + \frac{(e_{15}^{''})^2}{\zeta_{11}^{''}}}{\rho_2}}$.

• Terms in the mechanical displacement $u_3^{'''}$ and electric potential $\phi^{'''}$ of the bottom piezoelectric layer:

$s = k\sqrt{1 - \frac{c^2}{c_3^2}}$, where c_3 denotes the phase velocity in the piezo-electric layer and is given by $c_3 = \sqrt{\frac{c_{44}^{'''} + \frac{(e_{15}^{'''})^2}{\zeta_{11}^{'''}}}{\rho_3}}$; $n = \frac{e_{15}^{'''}}{\zeta_{11}^{'''}}$.

• Expressions in the matrix for the dispersion relation:

$\Gamma = [\Gamma]_{ij}$
$\Gamma_{11} = -(\mu_T + 2\mu_L a_2^2 - 2\mu_T a_2^2)(\frac{M_1 kH_1}{2}\cos(\frac{kH_1}{2}\sqrt{M_1^2 - 4M_2}) - \sin(\frac{kH_1}{2}\sqrt{M_1^2 - 4M_2})$
$+2(\mu_L - \mu_T)a_1 a_2 ikH_1 \cos(\frac{kH_1}{2}\sqrt{M_1^2 - 4M_2}))$,
$\Gamma_{12} = -(\mu_T + 2\mu_L a_2^2 - 2\mu_T a_2^2)(\frac{M_1 kH_1}{2}\sin(\frac{kH_1}{2}\sqrt{M_1^2 - 4M_2}) + \cos(\frac{kH_1}{2}\sqrt{M_1^2 - 4M_2})$
$+ 2(\mu_L - \mu_T)a_1 a_2 ikH_1 \sin(\frac{kH_1}{2}\sqrt{M_1^2 - 4M_2}))$,
$\Gamma_{21} = -(\mu_T + 2\mu_L a_2^2 - 2\mu_T a_2^2)(\frac{M_1 kH_1}{2}\cos(\frac{kH_1 H_2}{2H_1}\sqrt{M_1^2 - 4M_2}) - \sin(\frac{kH_1 H_2}{2H_1}\sqrt{M_1^2 - 4M_2})$
$+ 2(\mu_L - \mu_T)a_1 a_2 ikH_1 \cos(\frac{kH_1 H_2}{2H_1}\sqrt{M_1^2 - 4M_2}))$,
$\Gamma_{22} = -\left(\mu_T + 2\mu_L a_2^2 - 2\mu_T a_2^2\right)\left(\frac{M_1 kH_1}{2}\sin\left(\frac{kH_1 H_2}{2H_1}\sqrt{M_1^2 - 4M_2}\right) + \cos\left(\frac{kH_1 H_2}{2H_1}\sqrt{M_1^2 - 4M_2}\right)\right.$
$\left.+2(\mu_L - \mu_T)a_1 a_2 ikH_1 \sin\left(\frac{kH_1 H_2}{2H_1}\sqrt{M_1^2 - 4M_2}\right)\right)$
$\Gamma_{23} = (c_{44}^{''} + \frac{e_{15}^{(2)2}}{\zeta_{11}^{''}})a_1 kH_1 \sin(a_1 kH_1 \frac{H_2}{H_1})$, $\Gamma_{24} = -(c_{44}^{''} + \frac{e_{15}^{(2)2}}{\zeta_{11}^{''}})a_1 kH_1 \cos(a_1 kH_1 \frac{H_2}{H_1})$,
$\Gamma_{25} = -e_{15}^{''} kH_1 e^{kH_1 \frac{H_2}{H_1}}$, $\Gamma_{26} = e_{15}^{''} kH_1 e^{-kH_1 \frac{H_2}{H_1}}$, $\Gamma_{31} = \Gamma_{21} - \alpha_1 kH_1 e^{-\frac{M_1 kH_1 H_2}{2H_1}}\cos(\frac{kH_1}{2}\sqrt{M_1^2 - 4M_2})$,
$\Gamma_{32} = \Gamma_{22} - \alpha_1 kH_1 e^{-\frac{M_1 kH_1 H_2}{2H_1}}\sin(\frac{kH_1}{2}\sqrt{M_1^2 - 4M_2})$, $\Gamma_{33} = \alpha_1 kH_1 \cos(a_1 kH_1 \frac{H_2}{H_1})$,
$\Gamma_{34} = \alpha_1 kH_1 \sin(a_1 kH_1 \frac{H_2}{H_1})$, $\Gamma_{43} = \frac{e_{15}^{''}}{\zeta_{11}^{''}}\cos(a_1 kH_1 \frac{H_2}{H_1})$, $\Gamma_{44} = \frac{e_{15}^{''}}{\zeta_{11}^{''}}\sin(a_1 kH_1 \frac{H_2}{H_1})$, $\Gamma_{45} = e^{kH_1 \frac{H_2}{H_1}}$,
$\Gamma_{46} = e^{-kH_1 \frac{H_2}{H_1}}$, $\Gamma_{53} = -(c_{44}^{''} + \frac{e_{15}^{(2)2}}{\zeta_{11}^{''}})a_1 kH_1 \sin(a_1 kH_1 \frac{H_3}{H_1})$, $\Gamma_{54} = (c_{44}^{''} + \frac{e_{15}^{(2)2}}{\zeta_{11}^{''}})a_1 kH_1 \cos(a_1 kH_1 \frac{H_3}{H_1})$,
$\Gamma_{55} = e_{15}^{''} kH_1 e^{kH_1 \frac{H_3}{H_1}}$, $\Gamma_{56} = -e_{15}^{''} kH_1 e^{-kH_1 \frac{H_3}{H_1}}$,
$\Gamma_{57} = -kH_1 e^{qkH_1 \frac{H_3}{H_1}}(c_{44}^{'''} q + e_{15}^{'''} pq)$, $\Gamma_{58} = kH_1 e^{-qkH_1 \frac{H_3}{H_1}}(c_{44}^{'''} q + e_{15}^{'''} pq)$, $\Gamma_{59} = -e_{15}^{'''} kH_1 e^{kH_1 \frac{H_3}{H_1}}$, $\Gamma_{5,10} =$

$e_{15}^{'''}kH_1e^{-kH_1\frac{H_3}{H_1}}$, $\Gamma_{63} = \Gamma_{53} - \alpha_2kH_1\cos(a_1kH_1\frac{H_3}{H_1})$, $\Gamma_{64} = \Gamma_{54} - \alpha_2kH_1\sin(a_1kH_1\frac{H_3}{H_1})$, $\Gamma_{65} = e_{15}^{''}kH_1e^{kH_1\frac{H_3}{H_1}}$, $\Gamma_{66} = -e_{15}^{''}kH_1e^{-kH_1\frac{H_3}{H_1}}$, $\Gamma_{67} = \alpha_2kH_1e^{qkH_1\frac{H_3}{H_1}}$, $\Gamma_{68} = \alpha_2kH_1e^{-qkH_1\frac{H_3}{H_1}}$, $\Gamma_{73} = \alpha_3kH_1\frac{e_{15}^{''}}{\zeta_{11}^{''}}\cos(a_1kH_1\frac{H_3}{H_1})$, $\Gamma_{74} = \alpha_3kH_1\frac{e_{15}^{''}}{\zeta_{11}^{''}}\sin(a_1kH_1\frac{H_3}{H_1})$, $\Gamma_{75} = kH_1e^{kH_1\frac{H_3}{H_1}}(\alpha_3+\zeta_{11}^{''})$, $\Gamma_{76} = kH_1e^{-kH_1\frac{H_3}{H_1}}(\alpha_3-\zeta_{11}^{''})$, $\Gamma_{77} = -pe^{qkH_1\frac{H_3}{H_1}}$, $\Gamma_{78} = -pe^{-qkH_1\frac{H_3}{H_1}}$, $\Gamma_{79} = -e^{kH_1\frac{H_3}{H_1}}$, $\Gamma_{7,10} = -e^{-kH_1\frac{H_3}{H_1}}$, $\Gamma_{85} = -\zeta_{11}^{''}kH_1e^{kH_1\frac{H_3}{H_1}}$, $\Gamma_{86} = \zeta_{11}^{''}kH_1e^{-kH_1\frac{H_3}{H_1}}$, $\Gamma_{87} = kH_1e^{qkH_1\frac{H_3}{H_1}}(-e_{15}^{'''}q + \zeta_{11}^{'''}pq)$, $\Gamma_{88} = kH_1e^{-qkH_1\frac{H_3}{H_1}}(e_{15}^{'''}q - \zeta_{11}^{'''}pq)$, $\Gamma_{89} = kH_1\zeta_{11}^{'''}e^{kH_1\frac{H_3}{H_1}}$, $\Gamma_{8,10} = -kH_1\zeta_{11}^{'''}e^{-kH_1\frac{H_3}{H_1}}$, $\Gamma_{97} = kH_1(c_{44}^{'''}q + e_{15}^{'''}pq)$, $\Gamma_{98} = -kH_1(c_{44}^{'''}q + e_{15}^{'''}pq)$, $\Gamma_{99} = e_{15}^{'''}kH_1$, $\Gamma_{9,10} = -e_{15}^{'''}kH_1$, $\Gamma_{10,7} = p$, $\Gamma_{10,8} = p$, $\Gamma_{10,9} = 1$, $\Gamma_{10,10} = 1$

Bikram Dholey,
Department of Mathematics,
Jadavpur University,
Kolkata
India.
E-mail address: bikram.dholey.563412@gmail.com

and

Kshitish Ch. Mistri,
Department of Mathematics,
Ramakrishna Mission Vivekananda Centenary College,
India.